JOURNAL OF APPLIED CRYSTALLOGRAPHY

ISSN: 1600-5767

journals.iucr.org/j

Orientations – perfectly colored

G. Nolze and R. Hielscher

J. Appl. Cryst. (2016). **49**, 1786–1802

JOURNAL OF APPLIED CRYSTALLOGRAPHY
ISSN 1600-5767

Orientations – perfectly colored

G. Nolze[a]* and R. Hielscher[b]*

[a]Federal Institute for Materials Research and Testing (BAM), Unter den Eichen 87, 12205 Berlin, Germany, and [b]Technical University Chemnitz, Reichenhainer Strasse 39, 09126 Chemnitz, Germany. *Correspondence e-mail: gert.nolze@bam.de, ralf.hielscher@mathematik.tu-chemnitz.de

Received 12 February 2016
Accepted 10 August 2016

Edited by G. Kostorz, ETH Zurich, Switzerland

Keywords: electron backscatter diffraction; color coding; symmetry groups; orientation description.

The inverse pole figure (IPF) coloring for a suitable evaluation of crystal orientation data is discussed. The major goal is a high correlation between encoding color and crystal orientation. Revised color distributions of the fundamental sectors are introduced which have the advantages of (1) being applicable for all point groups, (2) not causing color discontinuities within grains, (3) featuring carefully balanced regions for red, cyan, blue, magenta, green and yellow, and (4) an enlarged gray center in opposition to a tiny white center. A new set of IPF color keys is proposed which is the result of a thorough analysis of the colorization problem. The discussion considers several topics: (*a*) the majority of presently applied IPF color keys generate color discontinuities for specifically oriented grains; (*b*) if a unique correlation between crystal direction and color is requested, discontinuity-preventing keys are possible for all point groups, except for $\overline{4}$, $\overline{3}$ and $\overline{1}$; (*c*) for a specific symmetry group several IPF color keys are available, visualizing different features of a microstructure; and (*d*) for higher symmetries a simultaneous IPF mapping of two or three standard reference directions is insufficient for an unequivocal orientation assignment. All color keys are available in *MTEX*, a freely available MATLAB toolbox.

1. Introduction

For a spatially resolved characterization of crystalline materials, orientation mapping performed, for example, in a scanning electron microscope by electron backscatter diffraction (EBSD) is a very efficient tool. This technique uses locally acquired Kikuchi patterns in order to assign the crystalline phase and derive the orientation **G** of the pattern-forming volume. Compilations of numerous applications derived over the years are given by Schwartz *et al.* (2000, 2009).

Because several hundred thousand individual orientation measurements can be collected during a single microstructure mapping, one of the major challenges is a suitable visualization of such an enormous quantity of orientation or misorientation data. A coloring of data is commonly used since it provides a visually compelling encoding of complex information. In order to ensure the quantitative character of this imaging tool, appropriate color keys are required which enable an unequivocal, semi-quantitative and meaningful description of a crystal's orientation by the encoding color.

The applied color key can be understood as representing the anisotropic distribution of any physical or chemical property of a crystalline phase. It indicates the variation of a property with changing crystal direction or orientation. Thus, an abrupt orientation change defines a grain or phase boundary and should preferably become visible by a remarkable color variation, at least for a crystal direction which is affected by the orientation change. *Vice versa*, sudden color changes are undesirable if no remarkable orientation

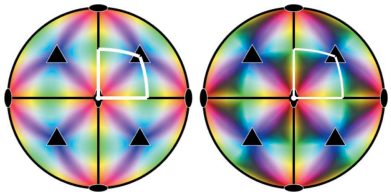

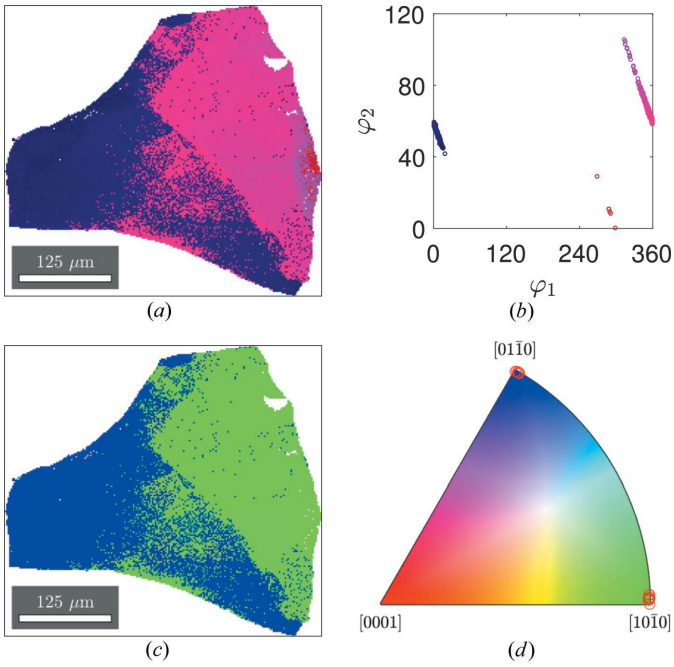

Figure 1
EBSD map of a single quartz grain. The color discontinuities in the Euler map (*a*) are caused by the jump of the Euler angle φ_1 from 360 to 0° (*b*). The color distribution of the key for $\bar{3}m$ (*d*) displays the reason for the color jump visible in the IPF-Y map (*c*): the reference directions (red circles) close to the symmetry-equivalent [10$\bar{1}$0] and [01$\bar{1}$0] are displayed either in green or in blue.

changes occur. Since this is a general problem in color encoding of crystal orientation data (*cf. e.g.* Fig. 1), this was the major driving force of the present work.

1.1. Coloring of Euler angles

A crystal orientation **G** is typically stored in terms of Euler angles, *e.g.* $\mathbf{G} = f(\varphi_1, \Phi, \varphi_2)$ following Bunge's notation (Bunge, 1982). It defines sequential rotations around three preselected reference axes, *e.g.* *Z*–*X*–*Z*, in order to bring a crystal from zero position into its orientation **G**. The easiest way to map orientation data is the encoding of the locally derived $(\varphi_1, \Phi, \varphi_2)$ by an assignment of each Euler angle to one of the primary colors red (R), green (G) and blue (B) (*cf.* Fig. 1*a*). The major disadvantage of this type of color encoding is the intricate interpretation of Euler angles (*cf. e.g.* Bunge, 1982; Kocks *et al.*, 1998; Randle & Engler, 2000). The three angles are unevenly distributed with respect to the orientation description, for example regarding the size of the angles themselves. This affects their visualized orientation sensitivity which mainly concerns the evaluation of misorientations from Euler angles. However, most problematic is the fact that regardless of the crystal symmetry Euler space encoding is affected by discontinuities in general, *i.e.* practically identical orientations can be encoded by clearly different colors. This shortcoming is the main reason why today's orientation maps are often only colored by Euler angles if other options are missing or improperly implemented by the applied software package.

A typical case of color discontinuities within crystal orientation maps is presented in Fig. 1(*a*), where the orientation-encoded color suddenly changes from violet to magenta within a single crystal. This happens because very similar orientations are defined by at least one totally different Euler angle, *cf.* the corresponding Φ slice of the Euler space in Fig. 1(*b*). Note that the comparatively large variations of φ_1 and φ_2 are only caused by a small misorientation of 2° maximum within the displayed quartz grain.[1] The result is an occasional appearance of speckled and/or two-colored grains within the orientation map, which precludes an unequivocal interpretation of orientation measurements since such color jumps typically can also indicate systematic misindexing, caused for example by any kind of pseudo-symmetry, or an improper setup of the measuring system.

1.2. Ideal coloring

An ideal color encoding can be defined in a very pragmatic way. Any crystal orientation should be described by a color such that the following conditions are met:

(1) Similar orientations are associated with similar colors.

(2) Different orientations are associated with different colors.

(3) The difference in color of two orientations corresponds to the size of the misorientation angle.

(4) The color definition is easily interpretable.

Unfortunately, it is mathematically impossible to construct a color encoding that satisfies at least the first two requirements. In other words, any color definition that unambiguously assigns colors to orientations will cause color jumps in orientation maps.[2]

1.3. Potential and challenges of IPF coloring

In order to overcome this mere visualization problem of exaggerated color jumps in Euler maps, in 1987 another coloring was introduced (Inokuti *et al.*, 1987). It is well known as inverse pole figure (IPF) coloring and is nowadays in vogue for the visualization of orientation data. The starting point is to fix a certain reference direction **r** as the vector of the specimen coordinate system, *e.g.* **r** parallel to the sample surface normal (**Z**) or the tilt axis (**X**), and to describe it as direction **h** of the crystal lattice by taking the crystal orientation **G** into account:

$$\mathbf{h} = \mathbf{G}^{-1}\mathbf{r}. \qquad (1)$$

In this way each orientation **G** is assigned to some crystal direction **h** – its pole point in the **r** inverse pole figure. Hence, by defining a colorization of the **r** inverse pole figure one obtains a color definition for the orientation **G**. In contrast to the coloring of Euler angles, this assignment is not one to one

[1] The maximum misorientation angle of 2° has been refined by pattern matching of experimental and simulated Kikuchi patterns (*cf.* Nolze *et al.*, 2016).

[2] Note that for misorientations $\Delta\mathbf{G}_{AB} = \mathbf{G}_A\mathbf{G}_B^{-1}$ between two grains A and B a color encoding is possible that satisfies the first two requirements (*cf.* Patala & Schuh, 2011; Patala *et al.*, 2012).

as orientations that have the same crystal direction **h** parallel to **r** are depicted by the same color.

The set of all possible but crystallographically non-equivalent **h** defines the fundamental sector of a symmetry group $\mathcal{P}$. In combination with an asymmetric color distribution this represents the $\mathcal{P}$-specific IPF color key. A color key that is presently used in commercial software for $\bar{3}m$, the Laue group symmetry of quartz (α-SiO_2), is exemplarily displayed in Fig. 1(*d*).

By way of illustration, in Fig. 1(*c*) the quartz grain is colored according to the crystallographic description **h** of $\mathbf{r} \parallel \mathbf{Y} = [010]$. The selection of $\mathbf{r} \parallel \mathbf{Y}$ is responsible for the name of the map: IPF-Y. Unexpectedly, within the single quartz grain the encoding of **h** shows color jumps comparable to those already displayed in the Euler angle map in Fig. 1(*a*). In order to indicate the reason for this surprising result, in the colorized inverse pole figure (Fig. 1*d*) the pole positions of $\mathbf{h} = \mathbf{G}^{-1}\mathbf{r}$ are inserted as red circles. They expose the fact that the symmetry-equivalent lattice directions $[10\bar{1}0]$ and $[01\bar{1}0]$ are misleadingly encoded by different colors.

Whether an IPF color key may cause color jumps in orientation maps or not becomes evident if the key is combined with the symmetry of the group, and plotted for all directions and not only for a single fundamental sector (Nolze, 2013). This is demonstrated in Fig. 2 for the 11 Laue groups considering IPF keys similarly used by the EBSD vendors. The color distributions projected on a surface of a cube or a hexagonal bipyramid visually prove that orientation maps free of color jumps may be guaranteed only for phases with the Laue group symmetry $m\bar{3}m$, $6/mmm$, $4/mmm$ or mmm, *i.e.* only for four out of 11. Inspecting the crystal systems it is conspicuous that all maps which visualize the IPF encoding of trigonal or rhombohedral phases (calcite, quartz, hematite *etc.*) can be affected by color jumps.

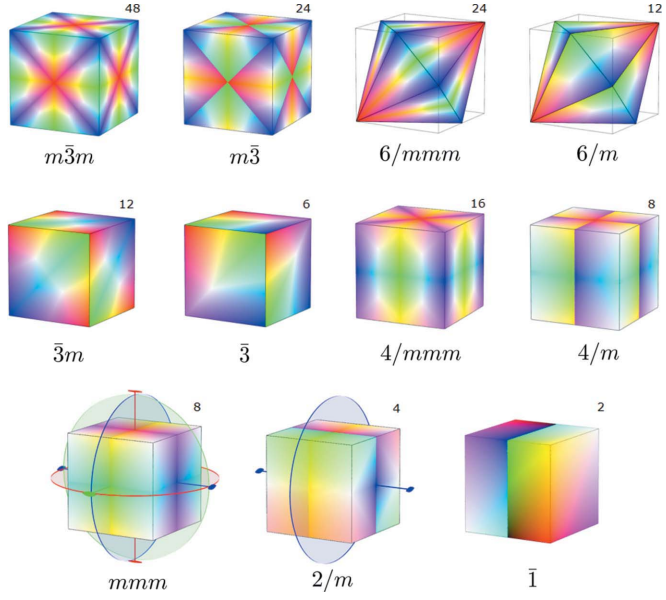

Figure 2
Standard color distribution for the 11 Laue groups. The projection onto the surface of a cube or a hexagonal bipyramid highlights the color discontinuities for $m\bar{3}$, $6/m$, $\bar{3}m$, $\bar{3}$, $4/m$, $2/m$ and $\bar{1}$. The small numbers at the right-upper position give the multiplicity of the respective group.

1.4. Key topics of this paper

The IPF map in Fig. 1(*c*) illustrates that, even if the size and shape of an IPF color key fulfill the requirements of a symmetry group, an improperly defined color distribution may generate physically meaningless discontinuities. Therefore, after some introductory remarks in §2, a generic approach for the generation of jump-free IPF color distributions is described which is applicable for the majority of point groups. Also, the typically neglected different setups of crystallographic basis vectors are considered, which are the result of an ambiguous alignment of symmetry elements, like $31m$ and $3m1$, or $\bar{4}2m$ and $\bar{4}m2$ (*cf.* Hahn, 1995, Table 10.1.2.2). It is only for $\bar{1}$, $\bar{3}$ and $\bar{4}$ that a simultaneously unequivocal and discontinuity-free assignment of colors is impossible, and so in the present paper $\bar{1}$, $\bar{3}$ and $\bar{4}$ are excluded from the discussion. Nevertheless, by way of illustration, for $\bar{1}$ a compromise is proposed which, however, does not enable an unequivocal assignment of a unique color to all **h**.

Given the fact that common EBSD systems exclusively use the Laue group symmetry of a phase for orientation determination, it might be surprising that we suggest the introduction of IPF keys for all 32 point groups. This has several reasons. On the one hand, we will show that even in the case of a centrosymmetric phase the IPF coloring enhances the ability to discriminate between differently oriented crystals by consideration of the symmetry of the respective maximal enantiomorphic subgroup. On the other hand, it is widely accepted that EBSD is not *a priori* a centrosymmetric technique (Baba-Kishi, 1991; Winkelmann & Nolze, 2015*a*; Nolze *et al.*, 2015), so that any limitation on Laue groups and their enantiomorphic subgroups is obsolete, and an adaptation of the respective imaging tools is required.

For good measure, in §3.1 we disprove the common belief that two or three IPF maps are sufficient for an unequivocal orientation identification. Exemplarily, we illustrate this by the identical coloring of non-equivalent transformation variants of γ-Fe precipitates.

All IPF keys are implemented in the freely available MATLAB (The MathWorks Inc., Natick, MA, USA) toolbox *MTEX-4.3* (Bachmann *et al.*, 2010). The equal-area projections of the color distributions for all $\mathcal{P}$ are given in Appendix *B*. All illustrations presented in this paper have been generated exclusively by *MTEX-4.3*. The corresponding documented script files are publicly available at http://mtex-toolbox.github.io/publications.html.

2. Advanced color keys for IPF color coding

The clear color jumps within the orientation map of a single quartz grain in Fig. 1 were the most annoying features of that map and the origin of this review. Therefore, this section has the aim of generating color distributions which guarantee a discontinuity-free IPF encoding of similar orientations. In

accordance with §1.4, we do not restrict ourselves to Laue groups but consider all 32 point groups including well accepted deviations in basis vector definitions.

2.1. Some general remarks

As postulated by equation (1), a general orientation is uniquely defined by a matrix $\mathbf{G}$ which maps the Cartesian reference coordinate system onto a Cartesian description of the crystal coordinate system, or *vice versa* (passive or active rotation; see *e.g.* Nolze, 2015). Despite describing the same orientation, the derived $\mathbf{G}$ might look diverse and therefore be described by different triples of Euler angles. This is caused by the unambiguous definition of crystallographic basis vectors as a consequence of the phase-inherent crystal symmetry.

2.1.1. Symmetry-specific orientation description. Using $\mathbf{W}_\mathcal{P}$ as symbol for a symmetry operator of the point group $\mathcal{P}$, an EBSD software package may return any of the orientations $\mathbf{GW}_\mathcal{P}$ as a possible indexing solution. The only restriction is that $\mathbf{W}_\mathcal{P}$ has to be a proper rotation $\mathbf{W}_\mathcal{P}^+$ with $\det \mathbf{W}_\mathcal{P}^+ = 1$, since these are the only operations that do not turn the describing right-handed coordinate system into a left-handed one. Therefore, orientation-equivalent directions to $\mathbf{h} = \mathbf{G}^{-1}\mathbf{r}$ are actually given by

$$(\mathbf{GW}_\mathcal{P}^+)^{-1}\mathbf{r} = (\mathbf{W}_\mathcal{P}^+)^{-1}\mathbf{G}^{-1}\mathbf{r} = (\mathbf{W}_\mathcal{P}^+)^{-1}\mathbf{h}. \quad (2)$$

From this it follows that even for centrosymmetric groups one can distinguish between $\mathbf{h}$ and $-\mathbf{h}$. It also explains why for a phase with symmetry $m\bar{3}m$, as described, for example, by Kocks *et al.* (1998), Randle & Engler (2000) and Nolze (2015), only 24 equivalent orientations are listed and not 48 as defined by the order of $\mathcal{P} = m\bar{3}m$.

It is particularly advantageous that the subset of all $\mathbf{W}_\mathcal{P}^+$ defines the maximal enantiomorphic subgroup $\mathcal{H}_\mathcal{P}$ of $\mathcal{P}$, so that for any point group $\mathcal{P}$ a well defined relationship for an orientation description exists. Thus one can conclude that for any non-enantiomorphic $\mathcal{P}$ the maximal enantiomorphic subgroup $\mathcal{H}_\mathcal{P}$ is used for the orientation description.

2.1.2. Laue group constraint. Even if a noncentrosymmetric phase is investigated, up to now EBSD systems have been designed to discriminate the signal with respect not to $\mathcal{P}$ but to the corresponding Laue group $\mathcal{S}$ only. This has its origin in the experimental observation that for the majority of phases deviations from a centrosymmetric diffraction signal are negligibly small (Friedel's rule).

By using the higher-symmetry Laue group $\mathcal{S}$, the symmetry operations $\mathbf{W}_\mathcal{S}^+ \in \mathcal{H}_\mathcal{S}$ of the maximal enantiomorphic subgroup $\mathcal{H}_\mathcal{S}$ of $\mathcal{S}$ are considered for orientation description. Hence, the following crystal directions have to be considered as equivalent:

$$(\mathbf{W}_\mathcal{S}^+)^{-1}\mathbf{h} = (\mathbf{W}_\mathcal{S}^+)^{-1}\mathbf{G}^{-1}\mathbf{r}. \quad (3)$$

Note that the maximal enantiomorphic subgroup $\mathcal{H}_\mathcal{S}$ of the Laue group $\mathcal{S}$ in general does not coincide with the point group $\mathcal{P}$ or with its maximal enantiomorphic subgroup $\mathcal{H}_\mathcal{P}$.

Depending on whether $\mathcal{P}$ is enantiomorphic, the multiplicity of $\mathcal{H}_\mathcal{S}$ is either the same as or twice the multiplicity of $\mathcal{H}_\mathcal{P}$. The size of the fundamental sector of $\mathcal{H}_\mathcal{S}$ is either the same as or half the size of the fundamental sector of $\mathcal{H}_\mathcal{P}$.

However, the hitherto used IPF coloring is exclusively related to the Laue group $\mathcal{S}$ of $\mathcal{P}$, *i.e.* the derived IPF maps always assign the same color for $\mathcal{P}$ non-equivalent directions $\mathbf{h}$ and $-\mathbf{h}$:

$$(\mathbf{W}_\mathcal{S})^{-1}\mathbf{h} = (\mathbf{W}_\mathcal{S})^{-1}\mathbf{G}^{-1}\mathbf{r}, \quad \mathbf{W}_\mathcal{S} \in \mathcal{S}. \quad (4)$$

2.1.3. Meaningful selections and suitable coloring. For a definition of an IPF color key the restriction to the fundamental sector of the symmetry group is beneficial, since it enables the encoding of symmetry-equivalent $\mathbf{h}$ by the same color. In order to prevent the assignment of different colors for practically symmetry-equivalent $\mathbf{h}$ one only has to ensure the use of a suitable color distribution for the respective fundamental sector of $\mathcal{P}$. Here, besides the asymmetry of the color distribution an additional condition is important. Two orientations $\mathbf{G}_1$ and $\mathbf{G}_2$ should be encoded by a similar color if their misorientation $\Delta\mathbf{G}_{1,2} = \mathbf{G}_1\mathbf{G}_2^{-1}$ is very small. This is what went wrong in the introductory example, since the $\mathbf{h}$ illustrated by red circles in Fig. 1(*d*) are close to the symmetry-equivalent $[10\bar{1}0]$ (green) and $[01\bar{1}0]$ (blue).

2.2. No symmetry: $\mathcal{P}$ = 1

In the case of no symmetry the fundamental sector is defined by all possible $\mathbf{h}$ and described by the entire projection sphere. Each point on the sphere is given by its polar coordinates (θ, ρ), where the polar angle θ runs on the upper hemisphere from 0 to 90° and on the lower hemisphere from 90 to 180°, and the azimuthal angle ρ runs from 0 to 360°. In order to define an asymmetric color distribution for the entire sphere we describe the color by the three values hue H, saturation S and lightness L, and set $H = \rho$, $S = 1$ and $L = \theta$ (*cf.* Fig. 3). Note that we are quite flexible in distributing the colors on the sphere. Some additional adaptations that lead to more balanced color distributions are discussed in Appendix *A*.

In the subsequent sections the color keys for all other crystal symmetries are defined by transforming the corresponding fundamental sectors in a suitable way onto the sphere and making use of the colorization that we have just discussed.

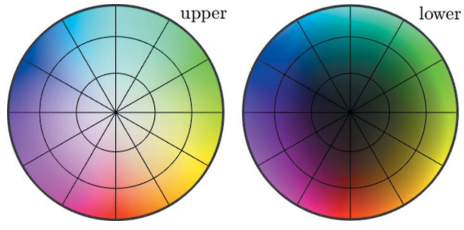

Figure 3
Colorization of the unit sphere (left: upper half; right: lower half) using fully saturated colors, *i.e.* $S = 1$ with hue H being the azimuth of a point on the sphere and the lightness L being the polar angle.

2.3. Mirror symmetry: $\mathcal{P} = m$

In the case of a single mirror symmetry m ($\equiv \bar{2}$) the fundamental sector is reduced to a hemisphere. After mirroring any color distribution of the fundamental sector onto the opposite hemisphere, no color discontinuities occur along the transition line between the two hemispheres. Thus, the color distribution given for the upper hemisphere in Fig. 3 is a suitable discontinuity-free color key for point group m.

An interesting question is whether it is possible to define a color key for point group m that contains not only all the bright colors from the upper hemisphere of Fig. 3 but also all the dark colors from the lower hemisphere. In fact it can be proven that this is impossible.

2.4. Standard color keys

The fundamental sector of a point group with order k higher than 2 can be chosen as either a spherical lune, a triangle or a square. In order to colorize these different shapes they are transformed onto the upper hemisphere such that the barycenter p of the sector is rotated into the north pole. For any point inside the sector the polar angle is defined as the distance to the barycenter p which is scaled in a way that the boundary of the sector has a polar angle of 90°, *i.e.* it is transformed onto the equator. The azimuth is given by the angle to the barycenter relative to some fixed vertex of the sector. The color of any **h** inside a fundamental sector is determined as description of the hue H by the azimuthal angle ρ, and of the lightness L by the polar angle θ of **h**, *cf.* §2.2. For illustration this is sketched in Fig. 4. Some more technical details about this mapping procedure are given in Appendix *A*.

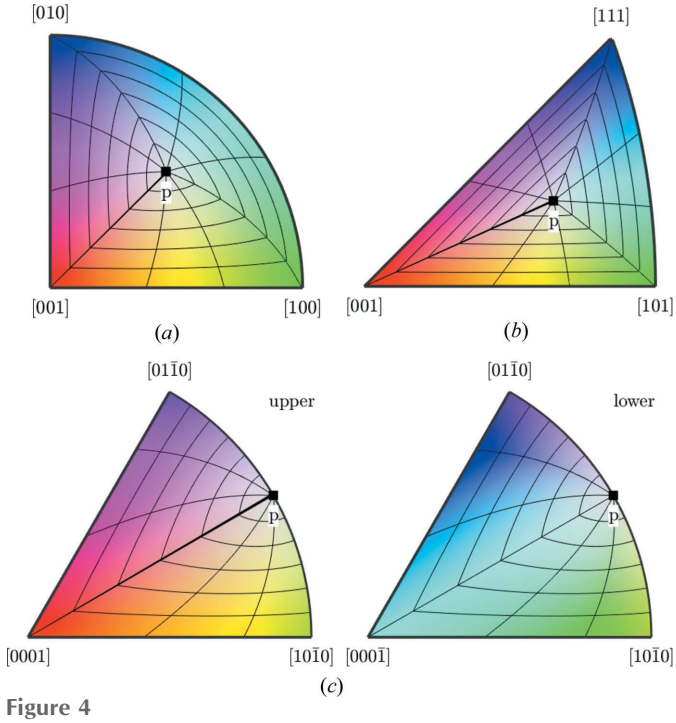

Figure 4
The fundamental sectors for orthorhombic symmetry *mmm* (*a*), cubic symmetry $m\bar{3}m$ (*b*) and trigonal symmetry $3m$ (*c*). For illustration, the barycenter p, grid lines for the polar angle at 15, 30, 45, . . . , 90°, and grid lines for the azimuthal angle at 0, 40, 80, . . . , 360° are overlaid. Because of symmetry, the color range only uses the upper half of the entire color range displayed in Fig. 3 (left). The color distribution of the hemisphere is transformed onto the spherical triangle by using polar coordinates.

lattice type	k	standard	k		extended			no
cubic	48	***m*$\bar{3}$*m***	24	432	***m*$\bar{3}$**			
	24	$\bar{4}3m$	12		23			
hexagonal	24	***6/mmm***	12	622	**$\bar{3}$*m***	**6/*m***		
	12	$\bar{6}2m$	6		32		$\bar{6}$	**$\bar{3}$**
	12	$6mm$	6			6		
	6	$3m$	3				3	
tetragonal	16	***4/mmm***	8	422	$\bar{4}2m$	**4/*m***		$\bar{4}$
	8	$4mm$	4			4		
orthorhombic /	8	***mmm***	4		222	**2/*m***		**$\bar{1}$**
monoclinic /	4	$mm2$	2			2		
triclinic	2	m	1				1	

Figure 5
Point groups differentiated by the type of the translation lattice, and whether they enable a discontinuity-free imaging by the standard or an extended color distribution. By color, we distinguish between centrosymmetric (Laue; bold black), noncentrosymmetric (blue), polar (bright green), enantiomorphic (red) and polar + enantiomorphic (dark green) groups. For $\bar{3}$, $\bar{4}$ and $\bar{1}$ neither the standard nor the extended color distribution is suitable. k defines the order of the respective groups.

We will refer to a color key generated as described in this section as a key with a 'standard' color distribution or as a 'standard color key'. Note that a standard color key contains either a dark or a bright center. Conversely, the color key for the point group 1 as defined in §2.2 contains both a bright and a dark center. Therefore, we will refer to it as a key with an 'extended' color distribution, or in brief as an 'extended color key'.

2.5. Fundamental sectors with reflection boundaries

As visible in Fig. 2, the standard color distribution is applicable for some Laue groups only. In fact the following result holds true: The fundamental sector of a point group can be colorized by the standard color distribution without discontinuities at the boundary of the fundamental sector if and only if all the boundaries are crystallographic mirror planes. The point groups which fulfill this condition are listed in Fig. 5 in the column 'standard'. Thus, the standard color distribution is applicable for all polar and non-enantiomorphic (green), but also some centrosymmetric (black) and noncentrosymmetric (blue) groups.

A more systematic analysis of the crystallographic symmetry shows that, if one describes R ($\mathrm{R} \in \mathrm{W}^+$) as the 'main' rotation axis,[3] all groups with mirror planes $\bar{2} \perp \mathrm{R}$ have to use the standard color distribution. Moreover, all groups containing additional twofold rotation axes fulfilling the

[3] For the cubic system the main rotation axes R are 3 or $\bar{3} \parallel \langle 111 \rangle$.

conditions (*a*) 2 ⊥ R and (*b*) 2 ⊥ $\overline{2}$ are uniquely described by the standard color distribution as well. Examples are $\overline{6}2m$ or $\overline{4}3m$, but not $\overline{4}2m$, as shown in Fig. 5. All remaining symmetry groups – except $\overline{1}$, $\overline{3}$ and $\overline{4}$ – are uniquely defined by the extended color distribution, as will be shown in §2.6. Fig. 5 sorts the groups with respect to the order k, *i.e.* all groups with the same order have the same size (but not shape) as the fundamental sector, *e.g.* 422, $\overline{4}2m$ and $4/m$, but also $4mm$ and mmm. For a certain group $\mathcal{P}$ a maximal subgroup relationship of index [2] is given by the groups behind (horizontal) and below (vertical) with the half-size of k. Index [i] defines the ratio between the orders for groups and subgroups. Transitions between point groups of different lattices are not straightforward so that only relationships within a lattice are easily recognizable. For example, the maximal subgroups of $6/mmm$ are $\overline{6}2m$ and $6mm$, but also 622, $\overline{3}m$ and $6/m$. For 32 the only subgroup of index [2] is 3.

2.6. Extended color keys

Fig. 2 shows that for seven Laue groups the application of the standard color distribution to a fundamental sector which is not entirely bounded by mirror planes leads to color discontinuities. This is again illustrated in Fig. 6(*a*) as an equal area projection for $\mathcal{P} = m\overline{3}$. Smooth color transitions through the reflection boundaries ∥ {100} occur, but along ∥ {110} partial color discontinuities are detectable.

A simple way to overcome these color discontinuities is to consider a definition that is invariant not only with respect to the point group $\mathcal{P}$ but also with respect to some supergroup $\mathcal{P}_+$, which is chosen such that its fundamental sector is entirely bounded by mirroring planes. In Fig. 5 for any point group $\mathcal{P}$ the minimal supergroup $\mathcal{P}_+$ with this property is listed in the same row in the column 'standard'. For $\mathcal{P} = m\overline{3}$ the matching supergroup is $m\overline{3}m$. The corresponding key in Fig. 6(*b*) is free of color discontinuities but ambiguous in the sense that symmetrically non-equivalent directions are associated with the same color.

For all point groups $\mathcal{P}$ listed in the column 'extended' of Fig. 5 the multiplicity is exactly twice the multiplicity of the matching supergroup $\mathcal{P}_+$ in the column 'standard'. Accordingly, the fundamental sector of $\mathcal{P}_+$ is half the size of the fundamental sector of $\mathcal{P}$. This allows us to colorize the half of the fundamental sector of $\mathcal{P}$ which coincides with the fundamental sector of $\mathcal{P}_+$ with a bright center using the barycentric coordinates to assign a color from the upper hemisphere (*cf.* §2.4). The remaining half will be colorized with a dark center, *i.e.* by using barycentric coordinates to assign a color from the lower hemisphere. The resulting key does not generate any color discontinuities since along the boundaries of the fundamental sectors the impact of the bright as well as of the dark center is zero and the colors along this connection zone are identical. For $m\overline{3}$ the so-derived key is displayed in Fig. 6(*c*). Following this approach one can define unambiguous and discontinuity-free keys for all point groups listed in the column 'extended' of Fig. 5.

The general procedure for encoding an orientation **G** by an extended color distribution is described as follows:

(1) Compute the crystal direction $\mathbf{h} = \mathbf{G}^{-1}\mathbf{r}$.

(2) Transform **h** into the fundamental sector of point group $\mathcal{P}$, *i.e.* find a symmetry operation W ∈ $\mathcal{P}$ so that **Wh** is inside the fundamental sector.

(3) Project **h** into the fundamental sector of the supergroup $\mathcal{P}_+$, *i.e.* find a symmetry operation $\mathrm{W}_+ \in \mathcal{P}_+$ such that $\mathbf{W}_+\mathbf{h}$ is inside the fundamental sector.

(4) Determine the coordinates (θ, ρ) of the barycenter for $\mathbf{W}_+\mathbf{h}$ according to §2.4.

(5) Check whether $\mathbf{W}_+\mathbf{h}$ and **Wh** coincide. If this is not the case, mirror (θ, ρ) to the lower hemisphere, *i.e.* replace θ by ($\pi - \theta$).

(6) Apply the triclinic IPF key as defined in §2.2 to assign a color to (θ, ρ).

2.7. The exceptional groups $\overline{1}$, $\overline{3}$ and $\overline{4}$

The fundamental sectors of these groups are topologically equivalent to the so-called two-dimensional projective space, the space of all lines passing through the origin of the three-dimensional Euclidean space (Coxeter, 1974). It can be

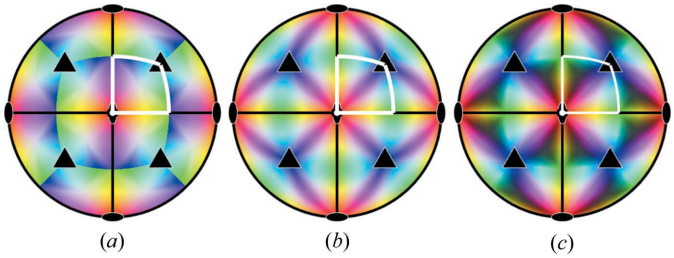

Figure 6
Different color distributions applied on the fundamental sector (white framed) of $\mathcal{P} = m\overline{3}$. The standard color distribution in (*a*) is defined according to §2.4. The color distribution in (*b*) corresponds to supergroup $m\overline{3}m$ and suffers from ambiguity. The extended color distribution in (*c*) is free of discontinuities and unambiguously assigns a single color to all symmetry-equivalent **h**.

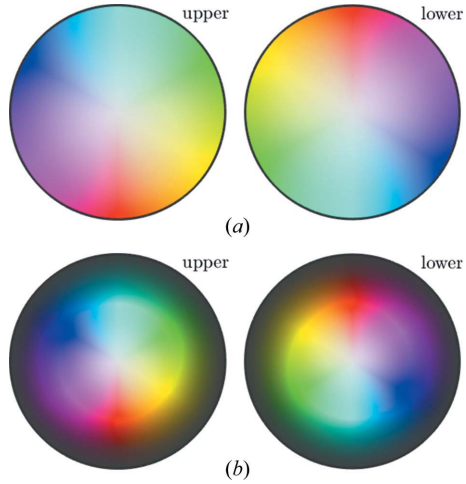

Figure 7
Two IPF keys for Laue group $\overline{1}$. An ambiguity-free IPF key with color jumps at the equator (*a*) and a color-jump-free IPF key with ambiguous directions around the equator (*b*).

mathematically proven that there is no jump-free embedding of these sectors into the three-dimensional space (Massey, 1959). In consequence, for $\overline{1}$, $\overline{3}$ and $\overline{4}$ any IPF distribution will either cause color jumps or assign the same color to crystallographically non-equivalent directions. For point group $\overline{1}$ the two possibilities are compared in Fig. 7. For the standard color distribution in (*a*) color jumps are generated along the entire equatorial line when moving from the upper to the lower hemisphere. The alternative color distribution in (*b*) prevents any color jump but assigns the same color (black) to all **h** defining the equatorial line.

For illustration, in Fig. 8 the symmetries of $\overline{3}$ and $\overline{4}$ are combined with the extended color distributions. Along the equatorial line, the upper and lower hemispheres always reflect a transition from blue to green. Only for the directions exactly between blue and green is the same color (turquoise) used for both hemispheres.

3. Applications

In the following we will discuss the advantages of the IPF coloring considering different symmetries, *i.e.* we will answer the question, which symmetry should be selected for which kind of orientation data visualization? First, an example will illustrate the limited uniqueness of the currently used IPF coloring.

3.1. On the uniqueness of IPF color encoding

Since an unequivocal interpretation of a crystal orientation **G** by only one reference direction **r** is impossible, usually several IPF maps are combined. However, it is common but unfortunately wrong to believe that with two or three IPF maps for **X**, **Y** and **Z** all orientations are uniquely color encoded. This is only true for the triclinic case. The reason is that for two reference directions $\mathbf{r}_1$, $\mathbf{r}_2$ and two crystal directions $\mathbf{h}_1$, $\mathbf{h}_2$ a fiber of orientation **G** with $\mathbf{G}\mathbf{h}_1 = \mathbf{r}_1$ and a fiber of orientation $\tilde{\mathbf{G}}$ with $\tilde{\mathbf{G}}\mathbf{h}_2 = \mathbf{r}_2$ intersect for triclinic symmetry in at most one orientation. For higher symmetries, however, also intersections between crystallographically equivalent fibers may occur.

The most basic counterexample appears for the monoclinic point group $\mathcal{P} = 121$ and the symmetrically not equivalent orientations $\mathbf{G}_1$ = (0, 0, 0°) and $\mathbf{G}_2$ = (180, 0, 0°). Both orientations have the same poles (001) and (00$\overline{1}$) in the **Z** inverse pole figure and the same poles (100) and ($\overline{1}$00) in the **X** inverse pole figure. Therefore, both orientations would be colored identically in the IPF-Z map as well as in the IPF-X map.

For a more practical illustration we selected the highest cubic crystal symmetry. In Fig. 9 the 24 orientation variants of γ-Fe are displayed, which are formed during transformation of a single grain of α-Fe according the Kurdjumov–Sachs model. The small maps of 6×4 squares depict each orientation variant. The lines between the squares indicate the grain boundaries (maximal misorientation angle 5°). Although the orientations of all variants are undoubtedly different, the existence of only three points within the inverse pole figure in Fig. 9(*e*) instead of the expected 24 verifies that several variants are described by the same **h**. In consequence, within the pole figure only three colors appear: red and two slightly different greens. Focusing on the red-colored variants in the IPF-Y map (middle), four of them are also identically colorized in IPF-X and IPF-Z, *i.e.* at least these variants cannot be distinguished. In order to recognize the related poles within the pole figure, they are labeled there as well.

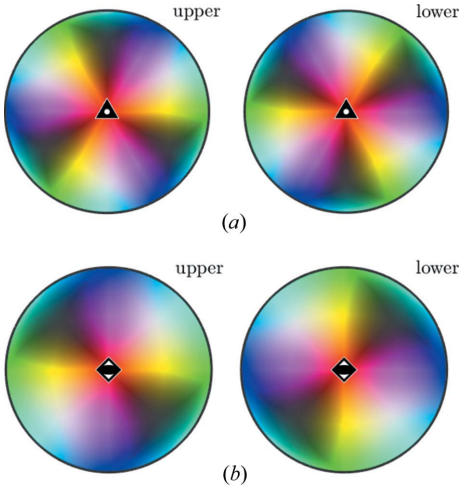

Figure 8
IPF keys for the Laue group $\overline{3}$ (*a*) and the noncentrosymmetric group $\overline{4}$ (*b*) with color jumps at the equator, *i.e.* at the same position on the circumference for the upper and for the lower hemisphere the same color should exist. Instead, an abrupt change from green to blue is visible.

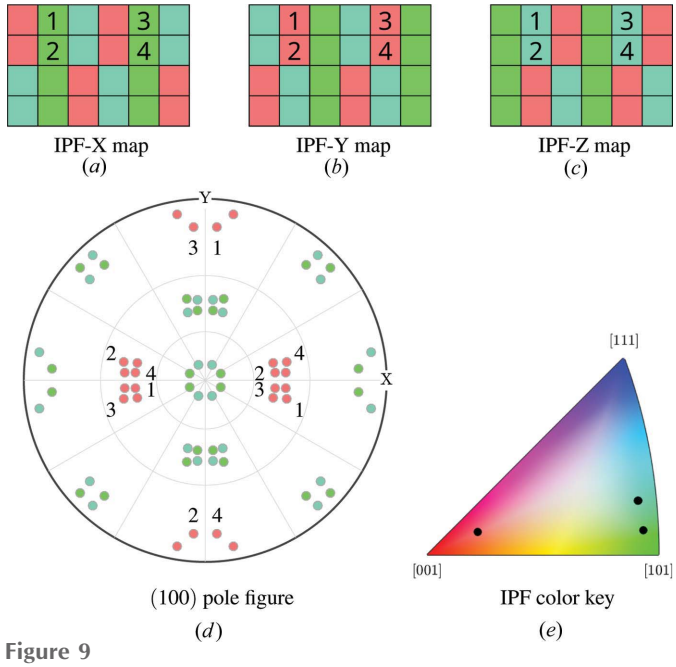

Figure 9
The 24 variants of the Kurdjumov–Sachs orientation relationship. The orientation variants are encoded for $\mathbf{r}_x$ (*a*), $\mathbf{r}_y$ (*b*) and $\mathbf{r}_z$ (*c*). The poles in the (100) pole figure (*d*) are colorized according to the coloring of $\mathbf{r}_y$. The IPF color key in (*e*) shows only three instead of the expected 24 pole positions for **h**, which proves that orientations of different variants are encoded by the same color and cannot be distinguished.

It becomes clear that with respect to the standard reference directions **X**, **Y** and **Z** the {100} poles appear rotation symmetric to each other. Applying the rotation symmetry $\parallel \mathbf{Z}$, variants 1 and 2, as well as variants 3 and 4, meet at the same pole positions.

For comparison, in Fig. 10 a slightly rotated pole distribution is represented, where the variants are no longer symmetrically aligned to **X**, **Y** and **Z**. As expected for general orientations, 24 different **h** appear within the inverse pole figure, and therefore the poles of all variants within the pole figure have different colors and can be clearly distinguished.

3.2. Laue *versus* point *versus* enantiomorphic group

As already theoretically sketched in §2.1, orientation data derived from Kikuchi patterns have to date by default been related to the Laue group $\mathcal{S}$ of the investigated phase. However, it can be beneficial to colorize orientation data with respect to the maximal enantiomorphic subgroup $\mathcal{H}_\mathcal{P}$ of the point group, or $\mathcal{H}_\mathcal{S}$ of the Laue group.

Therefore, for a systematic discussion of an IPF coloring three different cases can be distinguished:

(1) the point group $\mathcal{P}$ is centrosymmetric, *i.e.* it is a Laue group,

(2) the point group $\mathcal{P}$ is enantiomorphic, *i.e.* $\mathcal{P}$ only contains proper rotations, and

(3) the point group $\mathcal{P}$ is neither a centrosymmetric nor an enantiomorphic group.

3.2.1. Encoding for centrosymmetric point groups. If the point group $\mathcal{P}$ is centrosymmetric, the common assumption of an automatic replacement of $\mathcal{P}$ by its Laue group is redundant. A coloring of **h** according to $\mathcal{P}$ is then absolutely permissible since no improper simplifications have been applied. The limitations of this orientation coloring have already been illustrated by the example of the transformation variants given in §3.1. In the case of a very symmetric orientation of the parent α-Fe grain, four variants cannot be distinguished using the color key $\mathcal{P} = m\bar{3}m$ (*cf.* Fig. 9).

On the other hand, according to the explanations briefly given in §2.1, the orientation of a centrosymmetric group is defined by $\mathrm{W}^+_\mathcal{P}$ describing the maximal enantiomorphic subgroup $\mathcal{H}_\mathcal{P}$. Therefore, for a maximal orientation visualization the color key of $\mathcal{H}_\mathcal{P}$ is most helpful. Since this key differs between **h** and $-\mathbf{h}$, it enhances the discriminability of crystal orientations.

This can be illustrated by comparing the color key of $\mathcal{P} = m\bar{3}m$ in Fig. 9 with the color key of $\mathcal{H}_\mathcal{P} = 432$ in Fig. 11. Using $\mathcal{H}_\mathcal{P}$, the IPF maps of two standard reference directions suffice to discriminate between all 24 variants. For the same symmetric alignment the inverse pole figure in Fig. 11(*d*) contains again all 24 variants, but the consideration of the enantiomorphic symmetry encodes them by six different colors, which explains the higher discriminability.

Summarizing the IPF coloring of a centrosymmetric phase one can state that there are two possible but non-equivalent possibilities:

(*a*) coloring with respect to $\mathcal{P}$, and

(*b*) coloring with respect to $\mathcal{H}_\mathcal{P}$.

The first is preferred for a simple coloring of a reference direction **r** in order to display any correlation of a parallel-

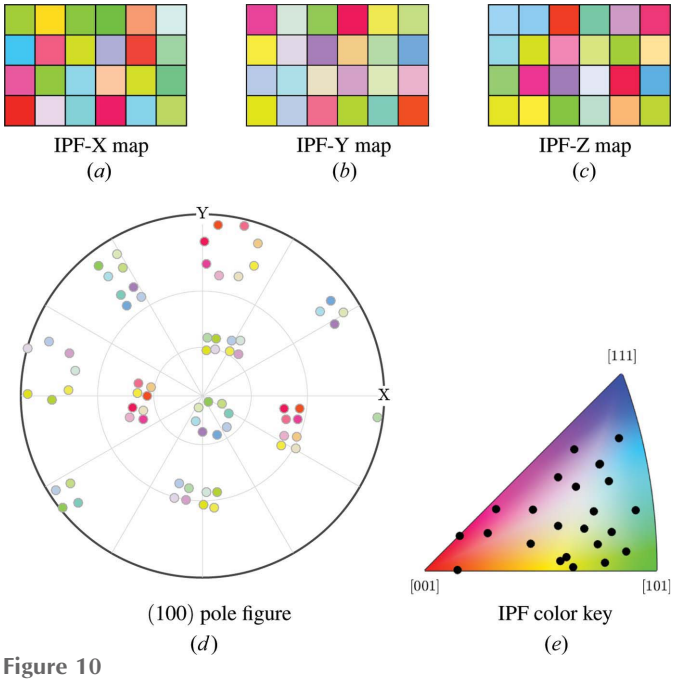

Figure 10
The 24 orientation variants of α-Fe (Kurdjumov–Sachs orientation relationship) assuming a general alignment of the parent γ-Fe grain. All colorized maps (*a*)–(*c*) as well as the (100) pole figure (*d*) and inverse pole figure for the reference direction $\mathbf{r} \parallel \mathbf{Y}$ (*e*) represent all variants by different colors.

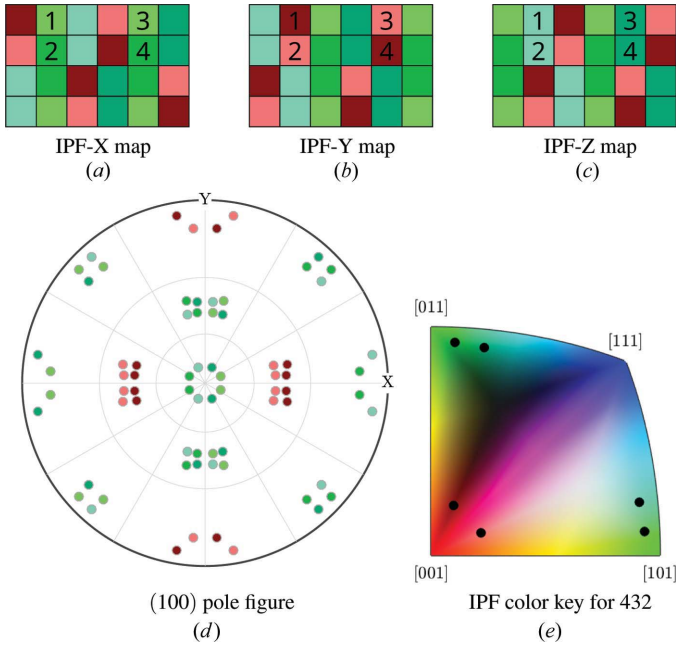

Figure 11
IPF maps for **X** (*a*), **Y** (*b*) and **Z** (*c*) displaying the 24 variants of the Kurdjumov–Sachs orientation relationship in the same alignment as given in Fig. 9. In (*d*) the color key for the enantiomorphic point group 432 is shown. The black dots define the six possible crystallographic descriptions of either **X**, **Y** or **Z**.

aligned loading axis, rolling or growth direction, temperature or concentration gradient, *etc*. to one or more crystallographic directions **h**. The orientation is here only a tool to determine all symmetry-equivalent **h** of $\mathcal{P}$. If a real visualization of the orientation is required, the better choice is the use of (*b*), since there any kind of symmetrization of orientation data is excluded.

3.2.2. Encoding for enantiomorphic point groups. In this case, the native symmetry of the considered phase contains only proper rotations. Although all presently existing commercial EBSD systems use the Laue group $\mathcal{S}$ for the indexing of Kikuchi patterns, the derived orientation description is always related to the maximal enantiomorphic subgroup $\mathcal{H}_\mathcal{S}$ (*cf.* §3.2.1). Since here $\mathcal{P} = \mathcal{H}_\mathcal{S}$, two color encodings are available: with respect to $\mathcal{P}$ and with respect to $\mathcal{S}$.

To illustrate the difference between them we reexamine the introductory example of quartz which is described by the enantiomorphic point group 321 but indexed according to $\bar{3}m1$. The centrosymmetric key for $\bar{3}m1$ is displayed in Fig. 12(*a*), and Fig. 12(*c*) shows the resulting entire color distribution after application of the symmetry on the color key.

Note that this key generated according to §2 is different from the one used in Fig. 1. The key of the enantiomorphic group 321 is displayed in Fig. 12(*b*). As a result of the halved order *k* caused by the maximal subgroup relationship, the size is twice that of (*a*). Fig. 12(*d*) shows again the color distribution after application of the point group symmetry. The entire color distributions in Figs. 12(*c*) and 12(*d*) both verify the discontinuity-free character of the newly defined color keys.

The most interesting question is how the different symmetries for the orientation description of quartz will affect the finally derived IPF maps. To this end, in Fig. 13 the IPF maps generated for different reference directions are compared according to the Laue group $\mathcal{S} = \bar{3}m1$ (left column) and the original enantiomorphic point group $\mathcal{P} = 321$ (right column). As expected from Figs. 12(*c*) and 12(*d*), both applied color keys successfully avoid the color jumps generated by the currently still used standard color key in Fig. 1. However, owing to the different color definitions for $\mathcal{S}$ and $\mathcal{P}$, the IPF

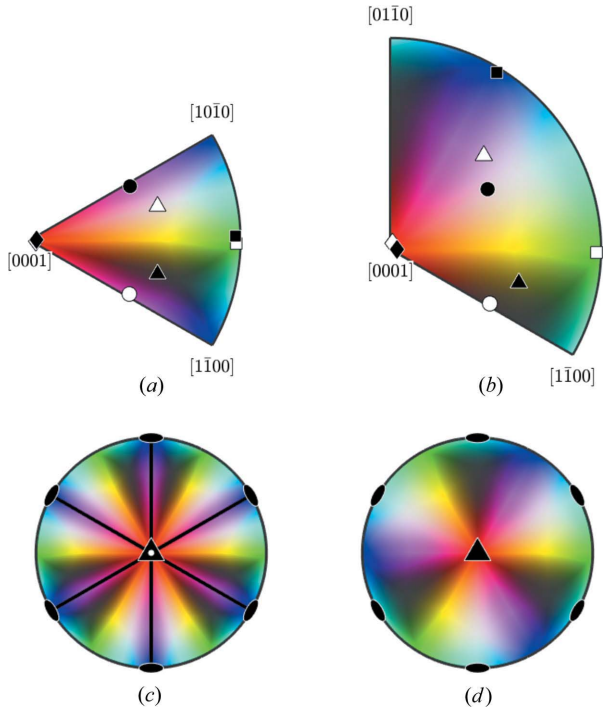

Figure 12
IPF keys for the fundamental sectors of the Laue group $\bar{3}m1$ (*a*) and its maximal enantiomorphic subgroup 321, *i.e.* ◆ ∥ $\langle 11\bar{2}0\rangle$ (*b*). The poles corresponding to the directions $\mathbf{r}_x$ (□), $\mathbf{r}_z$ (◇), $\mathbf{r}_1$ (○) and $\mathbf{r}_2$ (△) are colored black for the host grain and white for the twinned inclusion. In (*c*) and (*d*) the equal-area projections of the entire color distributions are given, overlaid by the symmetry elements of the respective groups.

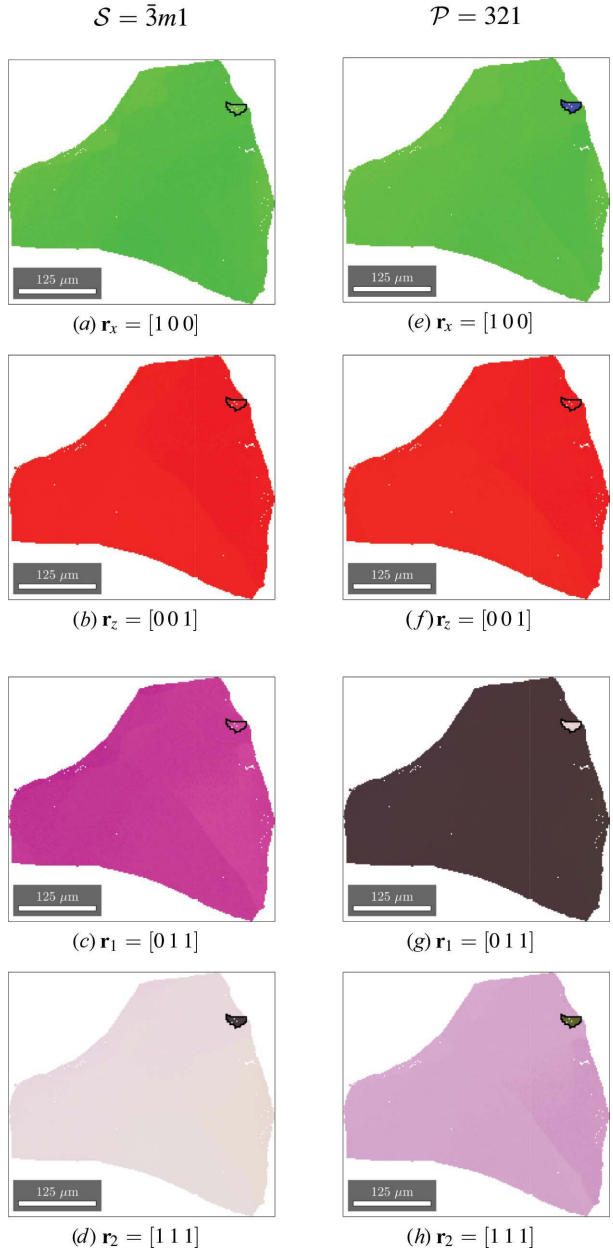

Figure 13
The quartz grain from Fig. 1 colorized by the adapted IPF key of $\mathcal{S}$ (left) and by the IPF key of $\mathcal{P}$ (right). The used color keys are given in Fig. 12. The different maps are color coding different reference directions. A small twin is marked by a black boundary.

maps of the two symmetries only appear similar for specific crystal orientations.

We focus on the small twin outlined by a black grain boundary at the top right in the IPF maps. Caused by a Brazil or Dauphiné law, the twin is surprisingly often encoded by almost the same colors as the host crystal. With respect to the color encoding of $\overline{3}m1$, the IPF maps of $\mathbf{r}_x$, $\mathbf{r}_z$ and $\mathbf{r}_1 = [011]$ are involved, and only for a general reference direction $\mathbf{r}_2 = [111]$ can the host and twin orientations be visually distinguished.

In contrast, by the use of the color key of 321, only the accidental alignment of $\mathbf{r}_z \parallel [0001]$, which is either the twin axis or part of the twin plane, leads to similar colors for host and twin. For all other reference directions the host and twin orientations are clearly discriminable.

A detailed observation of $\mathbf{h} = \mathbf{G}^{-1}\mathbf{r}$ projected in the IPF in Fig. 12 can explain this phenomenon more clearly. First, we concentrate on the IPF of $\overline{3}m1$ (*a*). The applied reference directions are described by different symbols: $\mathbf{r}_x$ (□), $\mathbf{r}_z$ (◇), $\mathbf{r}_1 = [011]$ (○) and $\mathbf{r}_2 = [111]$ (△). The presentation shows that the host (black symbols) and twin orientations (white symbols) are here encoded by nearly the same color since their poles are given by practically identical directions $\mathbf{h}_x$, $\mathbf{h}_z$ and $\mathbf{h}_1$. The reason is that for some of the chosen reference directions the symmetry along the circumference of the IPF key accidentally fits to the symmetry of the Brazil and Dauphinè law. In general, if a reference direction $\mathbf{r}$ is close to the peripheral zones of the fundamental sector, the host grain and twin will be colorized by the same color, because of the newly introduced symmetry property of the color distribution along the periphery. If a reference direction occupies a general direction $\mathbf{h}$ (△), a different color encoding of both host and twin orientations is also possible for a Laue-group-related coloring (*cf.* Fig. 13*d*). Since in a polycrystalline material practically any orientation can appear, a certain probability exists that reference directions of differently orientated grains are aligned along or close to the peripheral zone of the fundamental sector and can no longer be distinguished by their color. Differently oriented grains become identically colored.

As a comparison, the positions of $\mathbf{h}$ in Fig. 12(*b*) are no longer mirror symmetrically aligned with respect to $\{1\overline{1}00\}$. Using the color key of the enantiomorphic group one can now also visually distinguish between the two twinned grains by their different colors (*cf.* Figs. 13*e*, 13*g* and 13*h*). The only exception is the IPF-Z map, where $\mathbf{r}_z$ is arbitrarily parallel to [0001] and therefore the host and twin are both red colored (*cf.* Fig. 13*f*).

Summarizing this case, phases with enantiomorphic symmetry can be color coded by their enantiomorphic symmetry, if this symmetry is recognizable. However, if the orientation description is based on the respective Laue group $\mathcal{S}$ the application of the enantiomorphic group $\mathcal{H}_\mathcal{S} = \mathcal{P}$ can be beneficial, as demonstrated by the twin of quartz, or also for the previous example of the transformation variants of γ-Fe. However, although $\mathcal{H}_\mathcal{S} = \mathcal{P}$ this does not mean that orientations described by W of $\mathcal{P}$ and by W^+ of $\mathcal{H}_\mathcal{S}$ are identical. They can be mirror symmetric, and thus orientation descriptions related to $\mathcal{P}$ and to $\mathcal{S}$ will not be congruent.

3.2.3. Encoding for neither centrosymmetric nor enantiomorphic point groups. Finally, we consider the case that a group is not centrosymmetric but contains improper rotations. We also presuppose a point-group-sensitive indexing procedure as demonstrated by Winkelmann & Nolze (2015*b*) using a suitable automated indexing of standard EBSD patterns of $A^{III}B^{V}$ semiconductors ($\mathcal{P} = \overline{4}3m$). This approach is based on a Hough-transformation-related orientation determination using the respective Laue symmetry $\mathcal{S} = m\overline{3}m$. The derived orientation descriptions are first related to the enantiomorphic subgroup $\mathcal{H}_\mathcal{S} = 432$, which is presently standard for all existing measuring systems.

The point-group-sensitive orientation evaluation is performed in a post-processing of pattern and orientation data. Since $\overline{4}3m$ does not contain any 90° rotation operation around ⟨001⟩, the two possible pseudo-solutions $(\varphi_1, \Phi, \varphi_2)$ and $(\varphi_1, \Phi, \varphi_2 + 90°)$ will be evaluated. This happens by pattern matching of the experimental Kikuchi signal with real-time-derived pattern simulations (Winkelmann *et al.*, 2007)

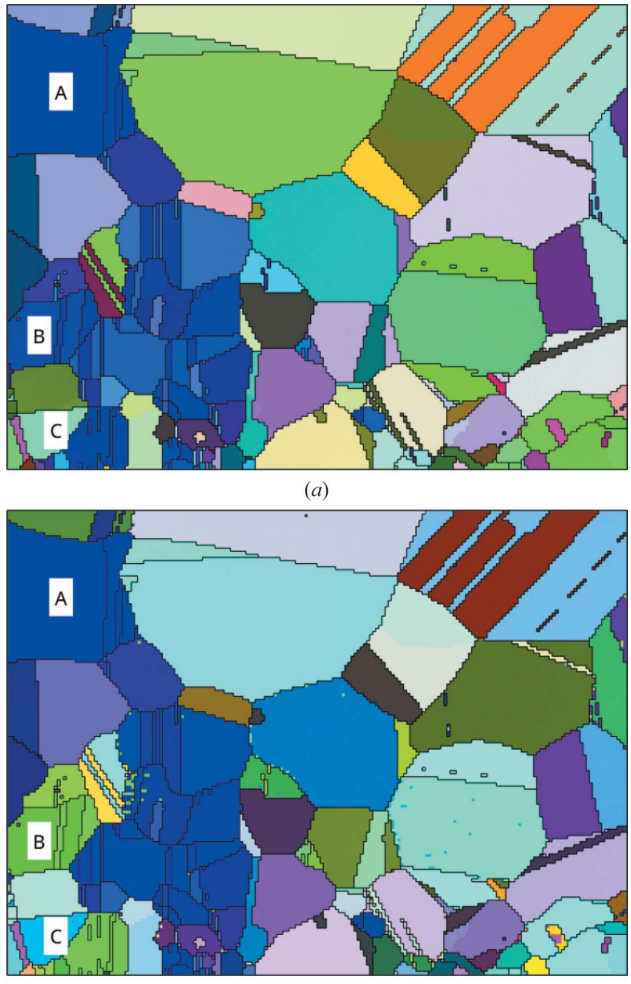

Figure 14
IPF map of a polycrystalline GaP microstructure indexed according to the Laue groups $m\overline{3}m$ (*a*) or to the point group $\overline{4}3m$ (*b*). The applied color keys are based on the enantiomorphic symmetry group 432 (*a*) or on 23 (*b*) (*cf.* Fig. 15).

and by including an orientation refinement. A better image correlation finally indicates the correct solution.

Since the orientation description is now based on the point group $\mathcal{P} = \bar{4}3m$, all Euler angles are related to the maximal enantiomorphic subgroup $\mathcal{H}_\mathcal{P} = 23$. Exemplarily, in Fig. 14 Laue-group-specific and point-group-specific orientation data of a polycrystalline microstructure of GaP are compared using the color keys of the respective enantiomorphic subgroups $\mathcal{H}_\mathcal{S} = 432$ (*a*) and $\mathcal{H}_\mathcal{P} = 23$ (*b*). The respective color keys are given in Figs. 15(*a*) and 15(*b*).

In both IPF-encoded orientation maps, A, B and C indicate three independent grains. Although the first map suggests that A and B are similarly aligned, while C is differently oriented, the computation of the misorientation angles $\Delta\varphi$ gives for grains A and B $\Delta\varphi = 78°$, between B and C $\Delta\varphi = 60°$, and for grains A and C $\Delta\varphi = 26°$. These values are much better represented by the color encoding in Fig. 14(*b*).

The reasons for the color differences of **h** are mainly controlled by the selected group symmetry. The multiplicities of 48 (for $\mathcal{S} = m\bar{3}m$), 24 (for $\mathcal{P} = \bar{4}3m$ but also $\mathcal{H}_\mathcal{S} = 432$) and 12 (for $\mathcal{H}_\mathcal{P} = 23$) indicate that with respect to the point group $\mathcal{P}$ the size of the fundamental sector has to be two times larger for $\mathcal{H}_\mathcal{P}$, half as large for $\mathcal{S}$ and identical for $\mathcal{H}_\mathcal{S}$. In order to make a comparison easier, in Fig. 15 an identical spherical segment is displayed which represents the fundamental sector of $\mathcal{H}_\mathcal{P}$ but consists, for example, for $\mathcal{S}$ of four fundamental sectors.

As already illustrated by the example of quartz, any transition to a higher-symmetry description is connected to some kind of loss of information which cannot be retrieved. Whereas [111] and [1$\bar{1}$1] with respect to $\mathcal{P} = \bar{4}3m$ are independent, the indexing according to $\mathcal{S} = m\bar{3}m$ does not enable us to distinguish between them anymore. Also the orientation description with respect to $\mathcal{H}_\mathcal{S} = 432$ distinguishes mathematically between **h** and −**h**, but not physically. A respective color mapping will not be able to express the polarity of [111] and [1$\bar{1}$1] (*cf.* Fig. 14*a*). In contrast, a transition to the lower-symmetry $\mathcal{H}_\mathcal{P} = 23$ keeps the capability to distinguish between [111] and [1$\bar{1}$1] (Fig. 14*b*), and it is also able to separate mirror-symmetric orientations.

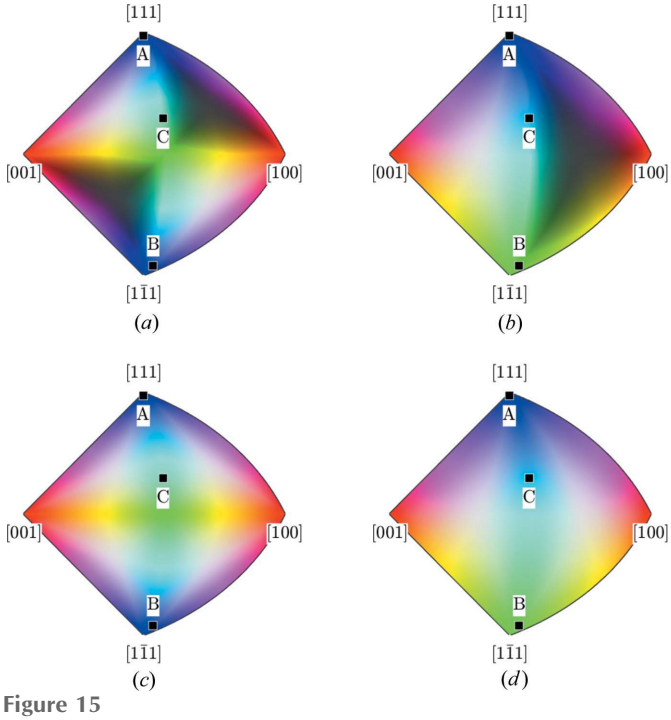

Figure 15
IPF keys for (*a*) $\mathcal{H}_\mathcal{S}$ = 432, (*b*) $\mathcal{H}_\mathcal{P}$ = 23, and the centrosymmetric point groups (*c*) $\mathcal{S} = m\bar{3}m$ and (*d*) $\mathcal{P} = \bar{4}3m$ with the mean orientations of the grains A, B and C annotated. For 432 and $\bar{4}3m$ the fundamental sector has been doubled and for $m\bar{3}m$ it has been quadrupled to cover the same sector as for 23.

In summary, for this most general case four possible IPF color keys are available. The use of $\mathcal{P}$ and $\mathcal{S}$ enables a crystallographic evaluation of a reference direction **r** as symmetry-equivalent **h**. The general use of $\mathcal{S}$ equalizes reverse directions which are perhaps required to distinguish polar properties. The application of the color keys of the enantiomorphic groups $\mathcal{H}_\mathcal{S}$ or $\mathcal{H}_\mathcal{P}$ is more suitable for a reliable visualization of crystal orientation data.

3.3. The agony of choice: appropriate color key selection

IPF coloring is more diverse than commonly assumed, and the currently applied coloring represents only one possibility with a limited validity. The previous discussion demonstrated that a meaningful coloring and a correct IPF key selection ultimately depend on the aim of visualization. Consistent for all IPF encodings is the fact that any orientation **G** is reduced to a description of a single reference direction **r** as crystallographically symmetry-equivalent $\mathbf{W}^{-1}\mathbf{h}$. This requires a critical analysis as to which group symmetry will be able to represent the extracted orientation information in the best or at least a meaningful way. If the aim of the typically only qualitative analysis is an easily visible correlation between a single reference direction **r** and an observable anisotropic alignment of crystals, the simplified use of $\mathcal{P}$ or even $\mathcal{S}$ is expedient. However, for a more orientation-related representation $\mathcal{H}_\mathcal{P}$ or even $\mathcal{H}_\mathcal{S}$ is the better choice.

The currently exclusively available IPF coloring using the Laue group $\mathcal{S}$ is only meaningful if the crystal structure is centrosymmetric ($\mathcal{P} = \mathcal{S}$), or an indexing with respect to the not centrosymmetric signal is impossible or of low reliability (pseudo-symmetry). There are alternative imaging tools available in software packages, like different kinds of misorientation mappings, but they do not map the orientation itself. The here-suggested IPF coloring using the fundamental sector of the enantiomorphic subgroup of $\mathcal{P}$ represents a very straightforward tool. It perfectly matches the practically omnipotent orientation description by Euler angles without having their disadvantage of generating discontinuities during Euler space coloring.

A new imaging opportunity and a potential gain in information arise in the case that the structure of a phase is not centrosymmetric, and the Kikuchi signal allows a differentiation between opposite directions **h** and −**h**, *cf.* the example of GaP. Every analytical system that postulates the validity of Friedel's law for EBSD is *a priori* lost. Even in the case that

one has a dataset containing point-group-sensitive orientation descriptions, they can only be processed by making them centrosymmetric first. Because of the discriminability between **h** and −**h**, point-group-related IPF keys enable us to distinguish between polar directions in crystals, and because of their definition between nonpolar directions also (Nolze *et al.*, 1990). Wherever the unacceptable symmetrization to the Laue symmetry limits an interpretation of observed phenomena, the point-group-symmetry-related interpretation of orientation data might be essential.

Nevertheless, as for the Laue-group-related imaging the application of the IPF key of the point group only describes the impact of **G** on **r** and not **G** itself.

4. Summary and conclusions

Current IPF coloring is severely limited. The presently offered fundamental sectors are for various reasons incomplete (only one axis setting available for each group, or keys are missing for low symmetries) and limited to the 11 Laue groups. Moreover, for seven of the 11 Laue groups the presently used standard color distribution generates discontinuities within grains, which are misinterpretable as orientation errors. In general, the limitation to Laue groups is unreasonable since EBSD is a technique that does not fulfill Friedel's rule. To overcome all of these problems a complete set of color keys has been derived, which do not generate exaggerated color jumps and produce a homogeneous color variation even in the case of a continuous change of orientation. This is demonstrated on the example of quartz.

It has been shown that for $\overline{1}$, $\overline{3}$ and $\overline{4}$ it is impossible to define color keys that do not generate color jumps in single grains. For $\overline{1}$ a possible workaround is given which, however, assigns crystallographically different directions to the same color.

The difference between IPF coloring of symmetry-equivalent reference directions using point or Laue group and of reference directions which originate from really symmetry-equivalent orientations using enantiomorphic (rotational) groups has been discussed.

With the example of a high-symmetry cubic transformation structure it has been demonstrated that, in contrast to common opinion, the combination of several IPF colorized maps is typically not a suitable method of displaying orientations unequivocally.

The color distribution within the keys (*cf. e.g.* Schwarzer & Sukkau, 2013; Nolze, 2013; Kayser, 2010) and sometimes also the shape of the fundamental sectors varies from definition to definition. Therefore, for a general interpretation of colorized IPF maps a standardization of size, shape and color distribution would be reasonable. The paper suggests a more regular distribution of colors in order to recognize orientation variations not only for specific colors. All color keys are implemented in the Matlab toolbox *MTEX 4.3*. Commented scripts that generate all figures but Fig. 2 of the paper can be found at http://mtex-toolbox.github.io/publications.html.

APPENDIX *A*
Color definition in color keys

This section covers the technical details in the definition of the HSV color values as described in §§2.2 and 2.4.

A1. An adapted hue gradient

One issue is that for linear hue the colors are unevenly distributed (see Fig. 16*a*). For this reason we do not go with constant speed through the hue but define a speed function $v(\rho)$ which is larger around the colors red, blue and green:

$$v(\rho) = 0.5 + \exp\left(-\tfrac{4}{7}[\rho]^2\right) + \exp\left(-\tfrac{4}{7}\left[\rho - \tfrac{2\pi}{3}\right]^2\right) + \exp\left(-\tfrac{4}{7}\left[\rho + \tfrac{2\pi}{3}\right]^2\right), \quad (5)$$

where $[\rho]$ is the projection of the angle ρ into the interval $[-\pi, \pi]$. The hue $h(\omega)$ as a function of the angle ω is now defined as

$$h(\omega) = \int_0^{\omega} v(\rho)\,\mathrm{d}\rho \Big/ \int_0^{2\pi} v(\rho)\,\mathrm{d}\rho. \quad (6)$$

A second issue is that in spherical triangles the distance $d(\rho)$ between the barycenter and the boundary might vary significantly with the angle ρ. As a consequence colors associated with directions that correspond to long distances, for example towards the vertices of the triangle, cover a larger area than colors associated with directions that correspond to small distances. In order to distribute the colors more uniformly we set the speed function $v(\rho)$, which we use for re-scaling the hue, proportional to the distance to the boundary $d(\rho)$, *i.e.*

$$v(\rho) = d(\rho)\left\{0.5 + \exp\left(-\tfrac{4}{7}[\rho]^2\right) + \exp\left(-\tfrac{4}{7}\left[\rho - \tfrac{2\pi}{3}\right]^2\right) + \exp\left(-\tfrac{4}{7}\left[\rho + \tfrac{2\pi}{3}\right]^2\right)\right\}. \quad (7)$$

Finally, we would like the three corners of a triangle to be associated with the colors red, green and blue. However, for extremely acute angled triangles the angles $\omega_1, \omega_2, \omega_3$ between the barycenter and the three corners may be very different. To compensate for this we normalize the speed function $v(\rho)$ such that

$$\int_0^{\omega_1} v(\rho)\,\mathrm{d}\rho = \int_{\omega_1}^{\omega_1+\omega_2} v(\rho)\,\mathrm{d}\rho = \int_{\omega_1+\omega_2}^{2\pi} v(\rho)\,\mathrm{d}\rho = 1/3. \quad (8)$$

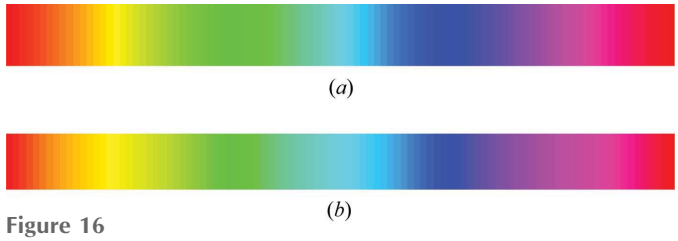

(*a*)

(*b*)

Figure 16
(*a*) Linear and (*b*) customized hue gradients.

A2. An adapted lightness and saturation gradient

The use of a linear map between the polar angle ρ and the lightness L has the effect that the white region in the IPF key is rather small when compared to the red, green or blue regions (*cf.* Fig. 1*d* or Fig. 17*a*). In this paper we used the following map for a more balanced key:

$$L = \lambda_L \frac{\rho}{\pi} + (1 - \lambda_L) \sin^2 \frac{\rho}{2}, \tag{9}$$

where the first summand is the linear map and the second summand is a map with a steeper gradient close to the poles. The parameter λ_L allows us to fine-tune between a small and a large white spot in the center. For $\lambda_L = 1$ we obtain the common linear map, whereas $\lambda_L = \frac{1}{4}$ gives a more balanced key (*cf.* Fig. 17*b*).

Using all saturated colors and, in particular, black and white for the colorization of orientations has the disadvantage that there is no color left that stands out and can be used for annotations, drawing grain boundaries or marking unindexed pixels. A possible workaround is not to use black and white for the center of the spherical triangles but bright and dark gray. This can be achieved by setting this saturation S as a function of the lightness L:

$$S = 1 - 2\lambda_S |L - 0.5|. \tag{10}$$

Here, the parameter λ_S controls how gray the center is colored. For $\lambda_S = 0$ we keep the white and black center, while $\lambda_S = 1$ results in bright gray and dark gray being identical. A good balance seems to be $\lambda_S = 0.25$, which was used in Fig. 17(*c*).

APPENDIX *B*
Discontinuity-free color distributions

Figs. 18–21 represent color distributions for the principally used point-group symmetries which are mapped on the upper and lower halves of a spherical surface and displayed in equal-area projection. The left column contains all groups whose symmetries are consistent with a standard color distribution. The right column lists all groups whose symmetry requires the extended color distribution. For convenience, the symmetry operators are overlaid. The respective color keys for each group are given by the sector defined by symmetry elements along the border. The presentation sequence follows the definition of point groups in *International Tables for Crystallography* (Hahn, 1995).

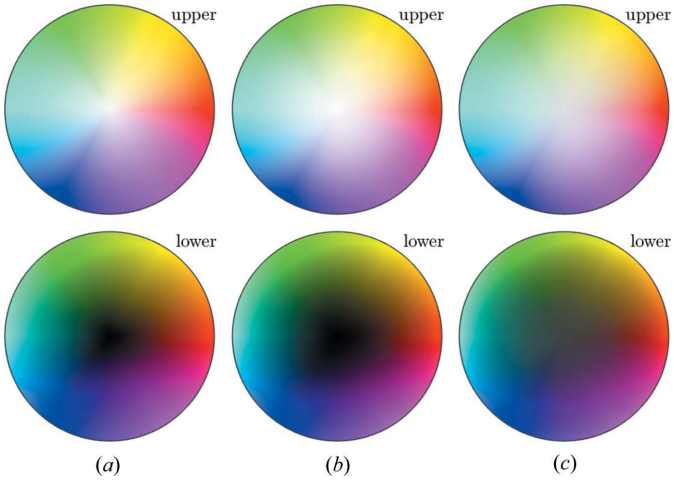

Figure 17
Triclinic IPF key with different scalings for lightness L and saturation S. (*a*) $\lambda_L = 1$, $\lambda_S = 0$, (*b*) $\lambda_L = 0.2$, $\lambda_S = 0$ and (*c*) $\lambda_L = 0.2$, $\lambda_S = 0.2$. The common linear scale is visualized in (*a*), while (*b*) displays a nonlinear lightness scaling and (*c*) displays nonlinear lightness in combination with lightness-dependent saturation.

Acknowledgements

We thank Aimo Winkelmann for providing a dataset demonstrating the point-group-sensitive indexing for the example of GaP.

References

Baba-Kishi, K. Z. (1991). *J. Appl. Cryst.* **24**, 38–47.
Bachmann, F., Hielscher, R. & Schaeben, H. (2010). *Solid State Phenom.* **160**, 63–68.
Bunge, H. J. (1982). *Texture Analysis in Materials Science: Mathematical Methods.* London, Boston: Butterworths.
Coxeter, H. S. M. (1974). *Introduction to Geometry.* New York: John Wiley & Sons.
Hahn, Th. (1995). Editor. *International Tables for Crystallography*, Vol A, *Space-Group Symmetry*, 4th ed. Dordrecht: Kluwer Academic Publishers.
Inokuti, Y., Maeda, C. & Ito, Y. (1987). *Trans. ISIJ*, **27**, 302–311.
Kayser, T. (2010). PhD thesis, TU Dortmund, Germany.
Kocks, U. F., Tomé, C. N. & Wenk, H. R. (1998). *Texture and Anisotropy: Preferred Orientations in Polycrystals and their Effect on Materials Properties.* Cambridge University Press.
Massey, W. S. (1959). *Pacific J. Math.* **9**, 783–789.
Nolze, G. (2013). *Microsc. Microanal.* **19**, 950–958.
Nolze, G. (2015). *Cryst. Res. Technol.* **50**, 188–201.
Nolze, G., Geist, V., Wagner, G., Paufler, P. & Jurkschat, K. (1990). *Z. Kristallogr.* **193**, 111–126.
Nolze, G., Grosse, C. & Winkelmann, A. (2015). *J. Appl. Cryst.* **48**, 1405–1419.
Nolze, G., Winkelmann, A. & Boyle, A. P. (2016). *Ultramicroscopy*, **160**, 146–154.
Patala, S., Mason, J. K. & Schuh, C. A. (2012). *Prog. Mater. Sci.* **57**, 1383–1425.
Patala, S. & Schuh, C. A. (2011). *Acta Mater.* **59**, 554–562.
Randle, V. & Engler, O. (2000). *Introduction to Texture Analysis: Macrotexture, Microtexture and Orientation Mapping.* Singapore: Gordon and Breach Science Publishers.
Schwartz, A. J., Kumar, M. & Adams, B. L. (2000). Editors. *Electron Backscatter Diffraction in Materials Science*, 1st ed. New York: Kluwer Academic/Plenum Publishers.
Schwartz, A. J., Kumar, M., Adams, B. L. & Field, D. P. (2009). Editors. *Electron Backscatter Diffraction in Materials Science*. New York: Springer Science+Business Media.
Schwarzer, R. & Sukkau, J. (2013). *Prakt. Metallogr. (Sonderband)*, **45**, 227–232.
Winkelmann, A. & Nolze, G. (2015*a*). *Ultramicroscopy*, **149**, 58–63.
Winkelmann, A. & Nolze, G. (2015*b*). *Appl. Phys. Lett.* **106**, 072101.
Winkelmann, A., Trager-Cowan, C., Sweeney, F., Day, A. P. & Parbrook, P. (2007). *Ultramicroscopy*, **107**, 414–421.

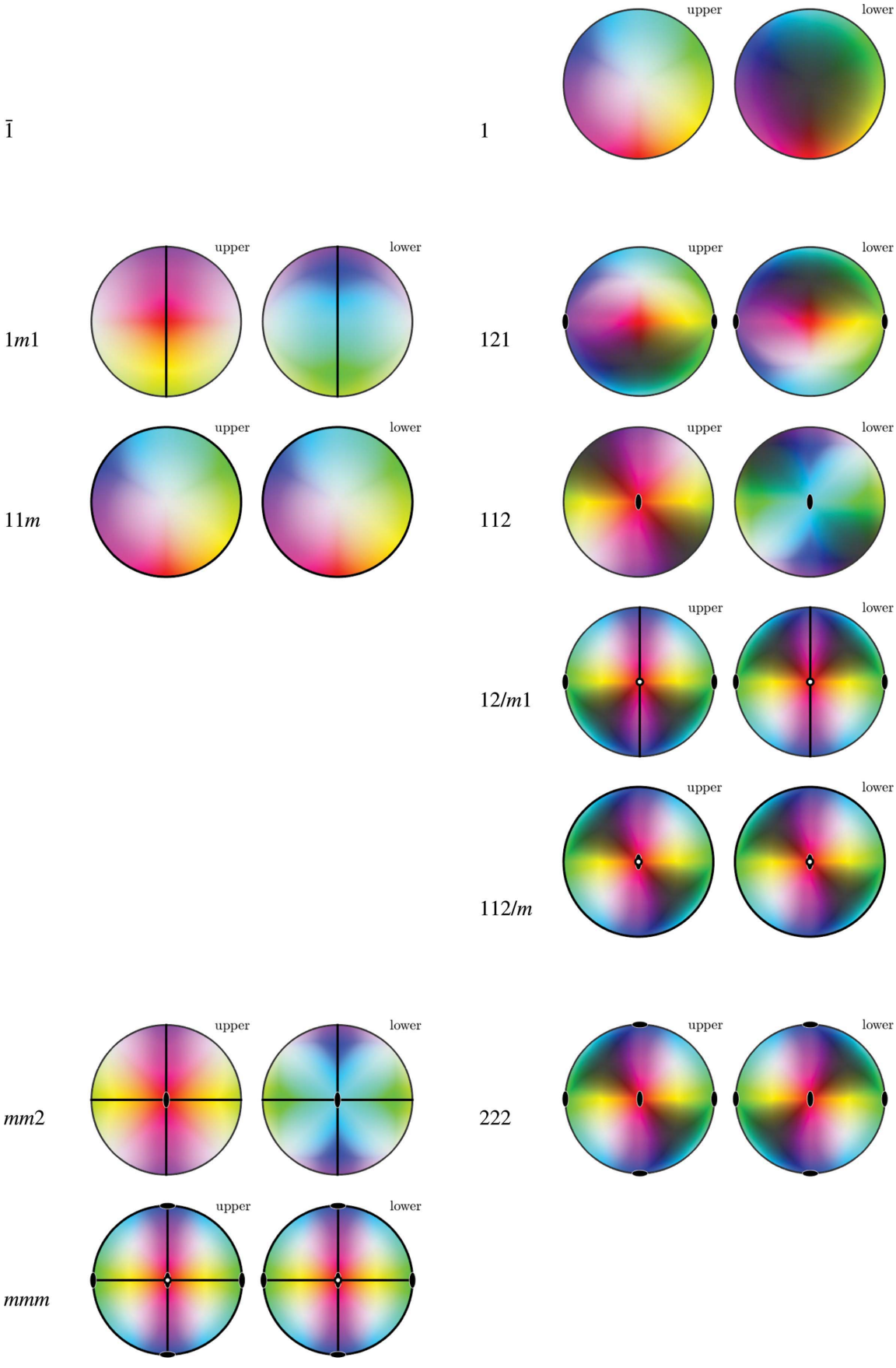

Figure 18
Color distributions (part 1).

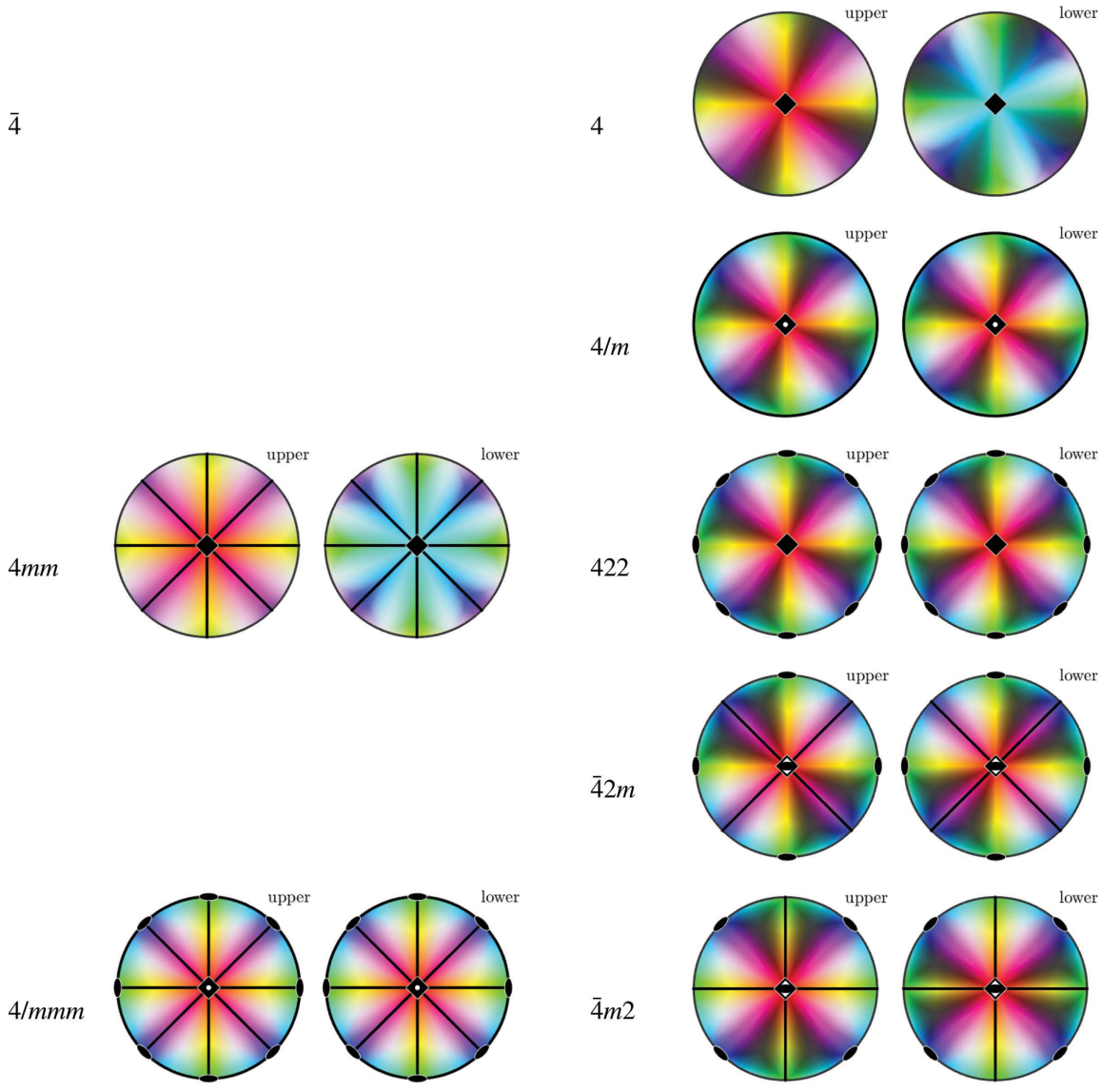

Figure 19
Color distributions (part 2).

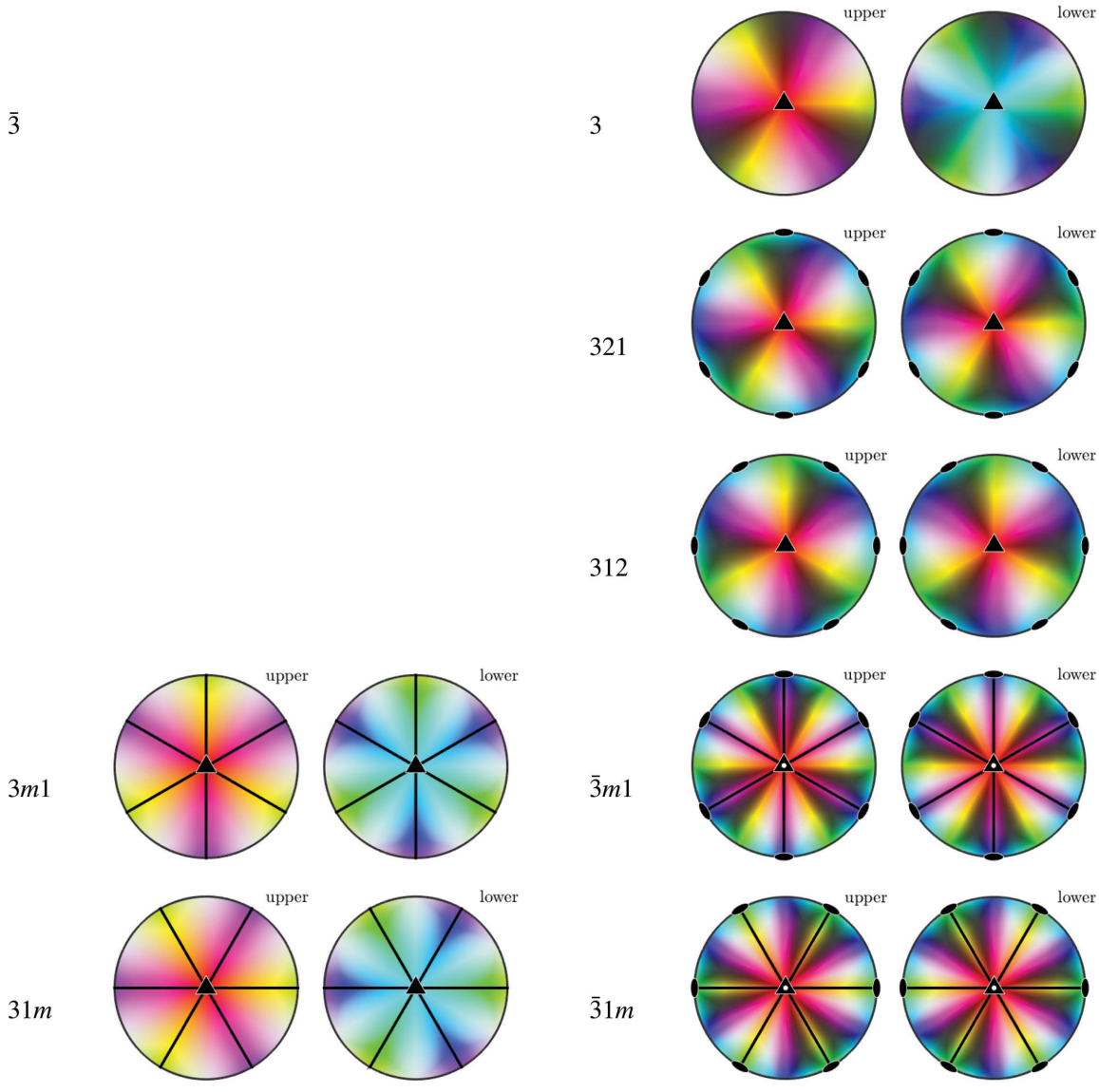

Figure 20
Color distributions (part 3).

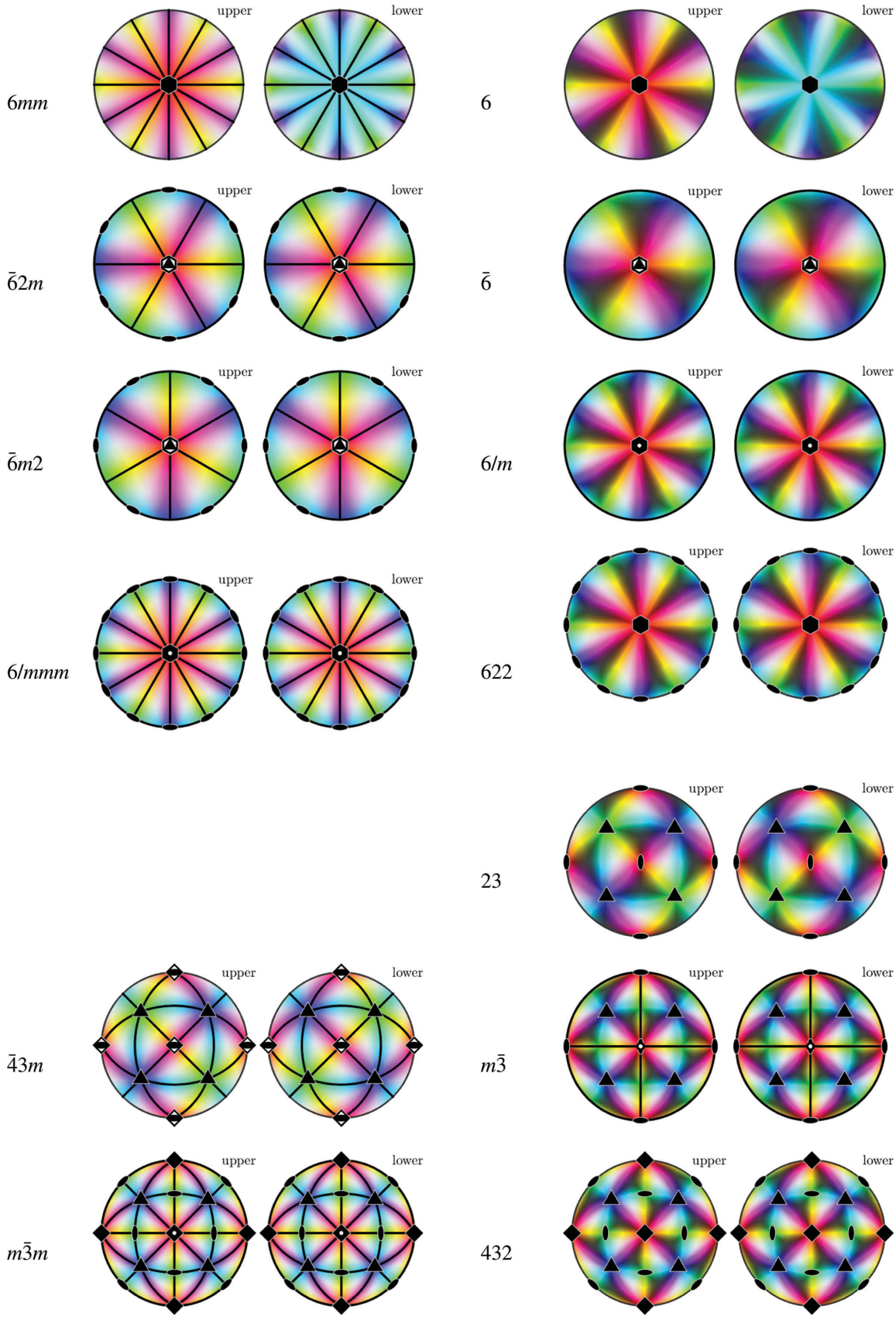

Figure 21
Color distributions (part 4).